Instrument Science Report WFPC2 2010-004

The Dependence of WFPC2 Charge Transfer Efficiency on Background Illumination

David A. Golimowski and John Biretta
December 01, 2010

ABSTRACT

We have examined the charge transfer efficiency (CTE) of WFPC2's CCDs near the end of mission as a function of background illumination. Internal lamps were used to flash the CCDs before or after external exposures of ω Cen to produce average background signals of 0–160 e^-. These signals span the natural sky backgrounds observed in ~99% of archived WFPC2 science images. Most of the stellar flux lost to poor CTE was recovered when the background signal was comparable to the average flux within the photometric aperture. Higher backgrounds contributed only more photon noise to the measurements. CTE losses from stars with aperture fluxes > 10^4 e^- are relatively small and insensitive to the background signal. For background signals > 10 e^-, WF4 showed better CTE than WF2 and WF3 at a statistically significant level. We also examined the efficacy of the latest formula for correcting CTE effects on WFPC2 aperture photometry obtained with the HSTphot and DAOPHOT software packages. The correction performs best on WF2 and WF3 photometry obtained with HSTphot; the residual error is ≤ 0.15 mmag/row (i.e., ≤ 0.06 mag at the centers of the CCDs) for almost all combinations of star and background signals. The correction does not perform as well on PC1 and WF4 photometry with background signals < 50 e^-. The DAOPHOT magnitudes of WF2 and WF3 sources are overcorrected by ~0.1 mmag/row relative to their HSTphot counterparts. However, the dispersion of the CTI-corrected DAOPHOT magnitude residuals for moderately bright stars imaged in all cameras is ~ 1/3 smaller than their HSTphot counterparts. These discrepancies probably reflect small differences between DAOPHOT's and HSTphot's aperture summing and sky-subtraction algorithms.

Operated by the Association of Universities for Research in Astronomy, Inc., for the National Aeronautics and Space Administration.

Introduction

An astronomical CCD camera must have good charge transfer efficiency (CTE) to ensure photometric fidelity across its field of view (FOV). The CTE of *HST's* CCD cameras degrades steadily over time because of continuous exposure to electrons and ions trapped in the Van Allen radiation belts, which permanently damage the CCD's silicon lattice and ionize its SiO_2 dielectric layer (Janesick 2001; Jones 2001). This radiation damage temporarily traps photoelectrons as they are clocked toward the output node, causing lost or deferred signal from an imaged source. The amount of lost or deferred signal is a function of time in orbit, the total signal from the source, the location of the image on the CCD, and the background illumination. Routine monitoring of WFPC2's CTE over 15 years with short external calibration exposures permitted assessments of all but the last condition because the sky background signal associated with these short exposures is typically less than ~10 e^- (Stetson 1998; Whitmore et al. 1999; Dolphin 2000a). The dependence of WFPC2's CTE (or, alternatively, its charge transfer inefficiency, CTI = 1 – CTE) on background signal should also be characterized, however, because a large fraction of WFPC2 science images were obtained under conditions of large sky background (Figure 1).

In this ISR, we investigate the efficacy of the WFPC2 CTI-correction formula derived by Dolphin (2009) when applied to WFPC2 images that have large sky background signals. This formula was derived using WFPC2 images recorded through August 2007 and an improved version of Dolphin's WFPC2 point-spread function (PSF) fitting stellar photometry package, HSTphot (Dolphin 2000b). Our investigation compares the CTI-corrected photometric measurements obtained from HSTphot with those obtained from the from the widely used DAOPHOT package (Stetson 1987).

Calibration Strategy and Observations

This study of the background dependence of WFPC2 CTE (Program 11031) is part of the suite of "close-out" calibration projects undertaken before the removal of WFPC2 from *HST* during Servicing Mission 4. Our observational strategy differs from that of the routine WFPC2 CTE monitor programs conducted between June 1999 and June 2007, in which images of the standard calibration field of ω Centauri (Walker 1994) were recorded at the central apertures of the WF2 and WF4 cameras in order to obtain contemporary images of the field oriented 180° apart with respect to the cameras' output nodes. For this study, we recorded images of the ω Cen field at two epochs (April 2007 and August 2007) using each of the central PC and WF apertures. These epochs closely

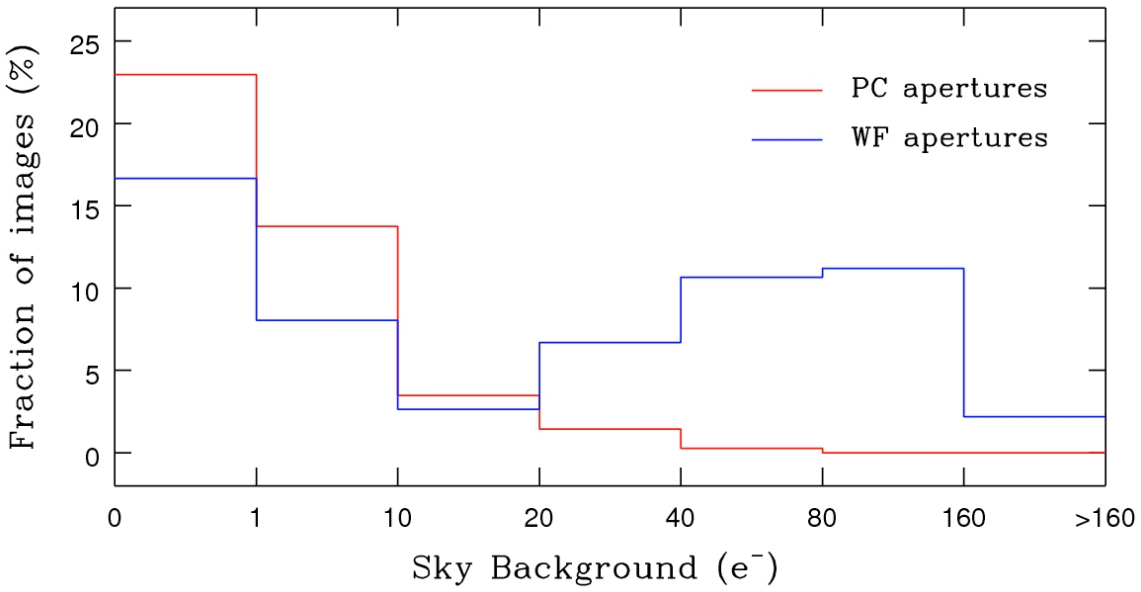

Figure 1. Percentages of archived WFPC2 science images with sky background signals in the designated ranges. The red histogram represents the images obtained with acquisition apertures PC1 and PC1-FIX. The blue histogram represents the images obtained with acquisition apertures WFn, WFn-FIX, WFALL, and WFALL-FIX, where n = 2, 3, 4. The distributions show that 88% of PC images have small background signals (< 10 e^-), while the number of WF images with large background signals (> 40 e^-) is approximately the same as those with small background signals.

followed adjustments of the temperature of WFPC2's electronics on 27 March 2007 and 14 August 2007, which were necessary to restore the normal function of a failing amplifier in WF4's signal-processing electronics (Dixon et al. 2007). Consequently, our images were not affected by the "WF4 anomaly." *HST's* roll angle was fixed at each epoch so that the orientations of the first and second epoch images were 138° apart. (The ideal roll angle offset of 180° was not possible because of scheduling constraints.) This strategy allowed the stars within each camera's FOV to be imaged twice at positions along CCD columns that are separated by up to ~700 rows (Figure 2).

Images of the ω Cen calibration field were recorded using the F814W filter and both analog-to-digital (A/D) conversion settings (ATD-GAIN=7 and ATD-GAIN=15). The F814W filter was chosen to mitigate photometric errors due to pixelation and to allow direct comparison with routine WFPC2 CTE monitoring programs. Two or three images were recorded at each gain setting using exposure times of 14 s and 100 s, respectively. Before reading each image, the CCDs were indirectly flashed by WFPC2's internal flat field (INTFLAT) lamps, which unevenly illuminated the inside of the closed shutter. The duration of the INTFLAT exposures was varied to produce average background signals of 20, 80, and 160 e^- in the WF cameras and 5, 20, and 40 e^- in the PC through the narrow-band F502N filter. Because the INTFLAT illumination was nonuniform, the

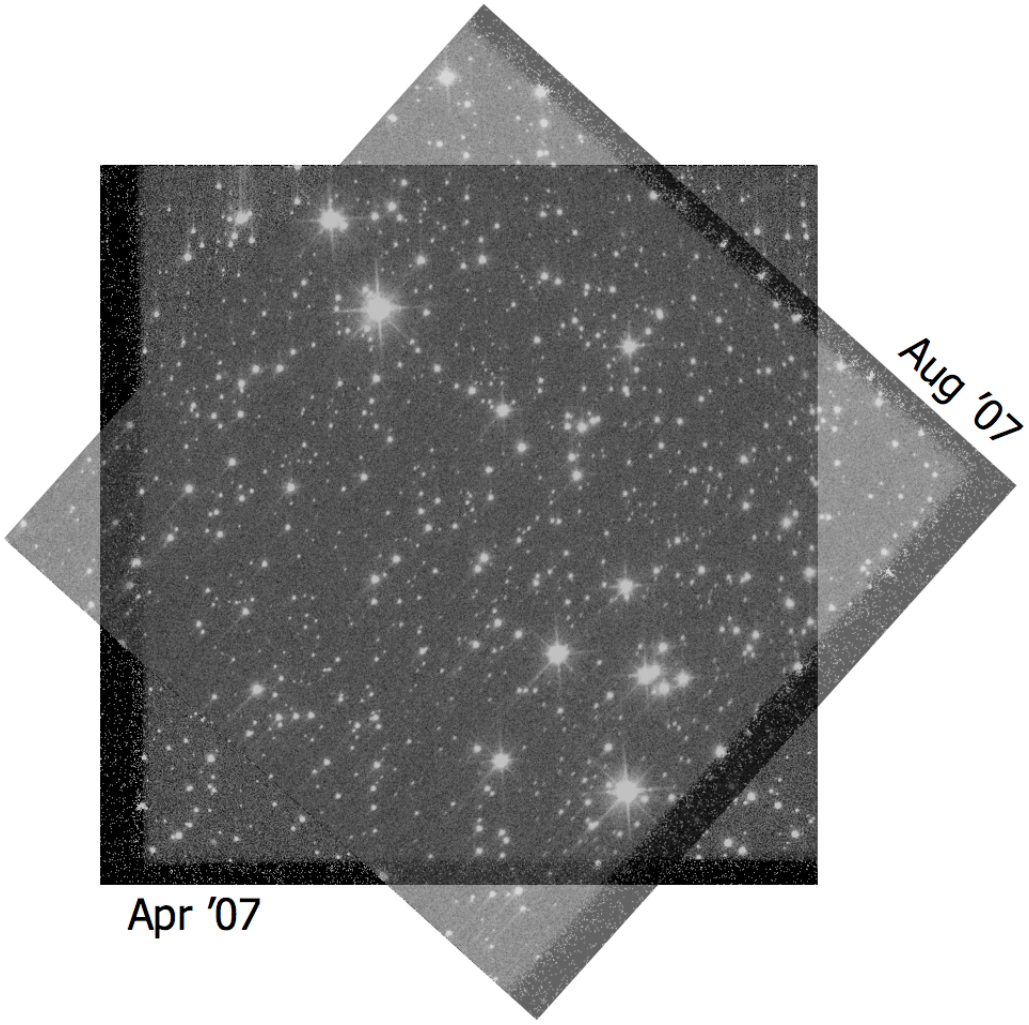

Figure 2. WF2 images of ω Cen calibration field obtained in April 2007 and August 2007. The August 2007 image has been rotated by 138° and superposed on the April 2007 image to show the number of stars present in both images and the positions of those stars relative to the readout node at each epoch. The readout node is located at the apex of the vignetted edges of the FOV.

background signals varied by 40–50% across the unvignetted FOV of each camera and by a factor of ~2.2 across the entire WFPC2 FOV (O'Dea et al. 1999). Unflashed exposures of ω Cen were also recorded to provide images with minimal background signal. A summary of the exposures recorded during each observing epoch is given in Table 1.

Collectively, the stars in ω Cen that were imaged by one or more WFPC2 cameras during both observational epochs provide a large set of differential photometry measurements that reflect the charge lost from WFPC2's CTI as functions of (1) the row separation between the two images of each star, (2) the intrinsic image brightness, and (3) the sky background level. Although the individual images of each star were recorded four

Table 1. Exposures recorded during each epoch (11–14 Apr 2007 and 21–23 Aug 2007)

Camera	ATD-GAIN (e^-/DN)	External exposure time (s)	INTFLAT exposure time (s)	Number of exposures
PC1	7	14	0	3
	7	14	5	2
	7	14	20	2
	15	100	0	3
	15	100	5	2
	15	100	20	2
	15	100	40	2
WF2	7	14	0	3
	7	14	3.5	2
	7	14	14	2
	15	100	0	3
	15	100	3.5	2
	15	100	14	2
	15	100	28	2
WF3	7	14	0	3
	7	14	3.5	2
	7	14	14	2
	15	100	0	3
	15	100	3.5	2
	15	100	14	2
	15	100	28	2
WF4	7	14	0	3
	7	14	6	2
	7	14	23	2
	15	100	0	3
	15	100	6	2
	15	100	23	2
	15	100	50	2

months apart, our observational baseline is sufficiently small compared with the temporal baseline over which Dolphin's CTI-correction formula is derived that our image pairs may be considered contemporaneous. We therefore consider our analysis to be an examination of Dolphin's formula at a single mid-2007 epoch. Unlike the routine WFPC2 CTE monitor programs, our analysis does not assume identical CTE for each WFPC2 CCD but instead permits an independent assessment of each camera.

Data Processing

Image Calibration and Reduction

All images were processed and calibrated though the OPUS pipeline using appropriate calibration reference files for the dates of observation. Subsequent data reduction and analysis was performed on the calibrated science images produced by the OPUS package *calwp2*, unless otherwise noted. No correction for geometric distortion was applied to the calibrated science images. Because our observations closely followed adjustments of WFPC2's electronics temperature in March 2007 and August 2007 (Dixon et al. 2007), the *calwp2* corrections for the WF4 anomaly were negligible.

From each set of exposures (defined by distinct combinations of observation date, camera aperture, external exposure time, and INTFLAT exposure time), we produced two average images, one of which was passed through a 2.5 σ cosmic-ray (CR) rejection filter. By subtracting the CR-rejected images from the individual exposures, we produced maps of all pixels affected by cosmic rays or other transient artifacts that were brighter than 10 σ above the local background. We produced a bad-pixel map for each exposure by marking all pixels that were saturated or flagged in the associated *calwp2* data quality (DQ) images as defective or invalid pixels. We also produced a hot-pixel map for each exposure by marking all pixels that were flagged in the DQ images as static or transient hot pixels. Finally, we produced bad-pixel and hot-pixel maps for each average image by summing the corresponding maps of its constituent exposures.

Photometry and Sample Selection

HSTphot was developed to provide more accurate photometry of crowded fields in undersampled WFPC2 images than can normally be obtained with generic PSF-fitting photometry packages (Dolphin 2000b). Photometry obtained with HSTphot is the basis for the WFPC2 CTI-correction formula developed by Dolphin (2000a, 2002, 2009). Ideally this formula would be applied exclusively to photometric data obtained with HSTphot, but Dolphin does not discourage its application to data obtained with other stellar photometry packages. To test the broader efficacy of Dophin's CTI correction, we identified and photometrically measured the stars in our ω Cen images using both HSTphot and the aperture mode of the general stellar photometry package DAOPHOT (Stetson 1987).

Using the *daofind* task in the IRAF DAOPHOT package, we identified all stars in the individual and CR-rejected images that had combined signal-to-noise (S/N) ratios ≥ 5 and

whose gaussian-fitted image widths were consistent with WFPC2 PSFs. We used the *phot* task to obtain the integrated fluxes of the stars in each camera within circular apertures of radius 3 pixels (for the PC) or 2 pixels (for the WF cameras), in conformity with the prescription for CTI correction defined by Dolphin (2000a, 2000b). The local sky background levels were determined from the median values of pixels within circular annuli of inner and outer radii 16 and 22 pixels (PC) and 9 and 11 pixels (WF cameras) centered on the stars, in rough conformity with the square "annuli" used by HSTphot (Dolphin 2000b). To protect our subsequent analysis against large systematic errors caused by the nonuniform INTFLAT illumination, we selected from the DAOPHOT catalogs for each camera only those stars whose associated sky backgrounds lay within 20% of an optimal background value determined for each combination of camera, external exposure time, and INTFLAT exposure time. Each optimal value was that which produced the largest number of star image pairs having that particular background signal at both observational epochs (Table 2).

We further winnowed the stars in our DAOPHOT catalogs by rejecting any star (1) having integrated S/N < 5 within the *phot* aperture, (2) located < 5 aperture radii from another star whose flux is > 1% that of the rejected star, (3) whose *phot* aperture contained a bad pixel, (4) whose *phot* aperture contained a CR or hot pixel whose signal was > 1% that of the rejected star, and (5) whose *phot* aperture intersected the region (*x*:*x*, *y*:*y*+CTE_TRAIL), where (*x*,*y*) are the pixel coordinates of CRs, hot pixels, or other stars, and CTE_TRAIL is the length of the deferred-charge trail caused by poor CTE. Ideally, CTE_TRAIL should be consistent with the *e*-folding time of charge release from long-term traps (~100 vertical charge transfers; Biretta & Kozhurina–Platais 2005), but the large numbers of CRs, hot pixels, and stars in our images make this value prohibitively costly to our sample size. Consequently, we chose CTE_TRAIL=20 as a compromise between photometric fidelity and statistical reliability. Despite these numerous rejection criteria, plenty of stars were retained for testing the efficacy of Dolphin's CTI-correction formula for each WFPC2 camera.

Conforming to the methodology of Dolphin (2000a), we scaled the fluxes of the surviving stars to the fiducial 0.″5 reference aperture using the tabulated WFPC2 encircled energy curves of Holtzman et al. (1995). We then applied the CTI corrections and photometric zero points of Dolphin (2009) to the individual and/or average magnitudes of each surviving star. We created a final DAOPHOT photometry catalog for each combination of camera, epoch, and INTFLAT setting that contained either the average magnitude of each surviving star (if none of the individual flux measurements was rejected) or a single measured magnitude (if one of the individual flux measurements was rejected).

Table 2. Optimal background signals (e^-) for each camera, INTFLAT duration, and external exposure time.[1]

INTFLAT duration[2]	External exp. time (s)	PC1	WF2	WF3	WF4
None	14	0.2	1.5	1.5	1.5
	100	1.5	7	7	7
Short	14	7	21	22	26
	100	10	29	29	32
Medium	14	20	80	79	92
	100	23	86	90	97
Long	14	…	…	…	…
	100	39	149	157	196

[1] Background signals include both INTFLAT illumination and external sky signal.

[2] Short, medium, and long durations correspond with INTFLAT exposure times for each camera listed in Table 1.

We generated a second set of photometric catalogs for each camera from the calibrated science images using HSTphot v.1.1 (updated on 8 September 2009), which is available at http://purcell.as.arizona.edu/hstphot/. In doing so, we masked bad pixels, removed hot pixels and CR artifacts, and coadded each set of exposures (as defined above) using the associated HSTphot tasks *mask, getsky, crmask, coadd,* and *hotpixels*. We then ran the task *hstphot* on each individual and CR-rejected image twice to obtain the magnitudes of all sources with combined S/N ≥ 5 with and without corrections for CTI and photometric zero point. Following the example of Dolphin (2009), we used the magnitudes obtained from small-aperture photometry to avoid potential systematic errors caused by fitting ideal model PSFs to faint, CTI-distorted images. We subjected the sources in the HSTphot catalog from each camera to the same winnowing criteria imposed upon the DAOPHOT sources, plus an additional criterion that the HSTphot object type flag must equal 1 (i.e., "good star"). As with the DAOPHOT results, we formed final HSTphot catalogs of uncorrected and CTI-corrected magnitudes for each camera, epoch, and INTFLAT setting based on the valid flux measurements of each surviving star.

The stars in the first-epoch catalogs were paired with the corresponding stars in the second-epoch catalogs using the *match* program written by Michael Richmond, which is based on the algorithm of Valdes et al. (1995) and available at http://spiff.rit.edu/match/. Table 3 lists the number of matched stars for each photometry package, camera, and gain setting. In all cases, the number of star pairs in our DAOPHOT and HSTphot catalogs differed by < 10%.

Table 3. Number of vetted and matched stars in each WFPC2 camera.

Gain	Target exp. (s)	Photometry package	PC1	WF2	WF3	WF4
7	14	DAOPHOT	39	190	196	173
		HSTphot	43	205	212	194
15	100	DAOPHOT	81	334	344	276
		HSTphot	85	341	340	300

A comparison of the photometry of stars appearing in both catalogs revealed that the integrated fluxes within the 3-pixel (PC) and 2-pixel (WF) circular apertures are ~33% and ~29% larger, respectively, in the DAOPHOT catalog than in the HSTphot catalog. We traced these large discrepancies to the different algorithms used by *hstphot* and IRAF's *phot* task when summing the fractional signals of square pixels that straddle the perimeters of the very small circular apertures. However, after applying the respective corrections to normalize the fluxes to the fiducial 0.″5 reference aperture (a precursory requirement for Dolphin's CTI correction), the discrepancies between the DAOPHOT and HSTphot measurements diminish to ~1% and ~5% for the PC and WF cameras, respectively. This convergence affirms that the aperture corrections of Holtzman et al. (1995) are appropriate when applying Dolphin's CTI correction to small-aperture DAOPHOT photometry.

Results and Analysis

Effect of sky background on WFPC2 photometry near end-of-mission

To assess the role of background illumination as a mitigator of photometric losses from poor CTE near the end of WFPC2's mission, we first qualitatively examined the differences in photometric magnitudes of stars of various intrinsic brightnesses as a function of background signal. Figure 3 shows for each WFPC2 camera the differences between the F814W magnitudes of stars with integrated aperture fluxes of ~100–65000 e^- obtained from 14 s (ATD-GAIN=7) external exposures taken at the same epoch (i.e., same field orientation), but with different levels of INTFLAT illumination and no subsequent CTI correction. The top and middle panels in each plot show that all the data is displaced above the Δmag = 0 lines, which indicates that even modest background signals of 10–80 e^- rectify the photometry of stars fainter than ~1000 e^- by 0.3–1.0 mag.

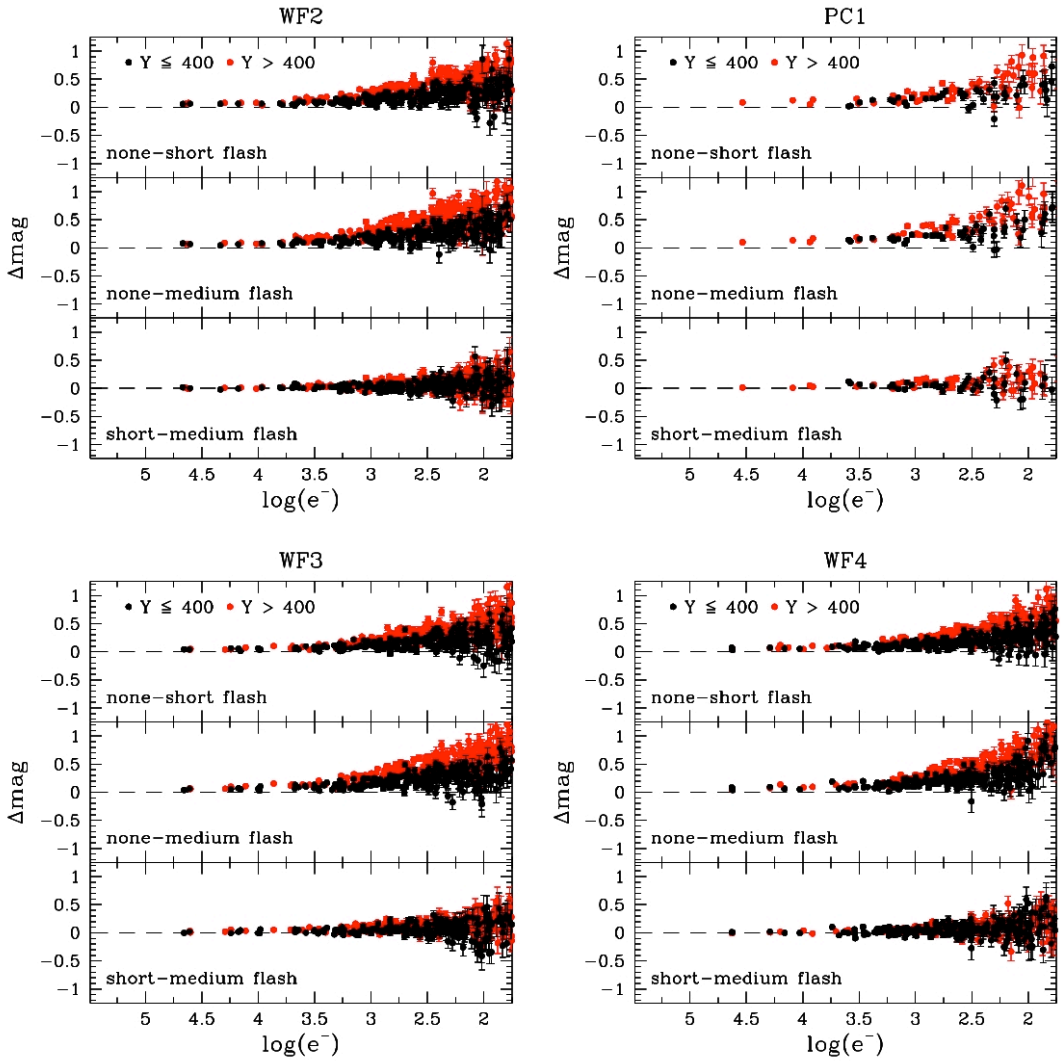

Figure 3. Effect of background signal on stellar photometry obtained with HSTphot for stars imaged in *(counterclockwise from upper right)* PC1, WF2, WF3, and WF4. Each plot has three panels showing the difference in magnitudes of unsaturated stars — without CTI correction — obtained from the 14 s (ATD-GAIN=7) F814W exposures taken with common image orientations and the following combinations of INTFLAT ("flash") exposures: *(top)* no flash and short flash, *(middle)* no flash and medium flash, and *(bottom)* short flash and medium flash. The background signals associated with each camera and flash level are given in Table 2. Data from stars located above and below the middle row (Y = 400) of each camera are shown as red and black points, respectively. The abscissae in each plot are the stars' integrated fluxes (in photoelectrons) obtained from the unflashed images using aperture radii of 3 pixels (PC) and 2 pixels (WF cameras).

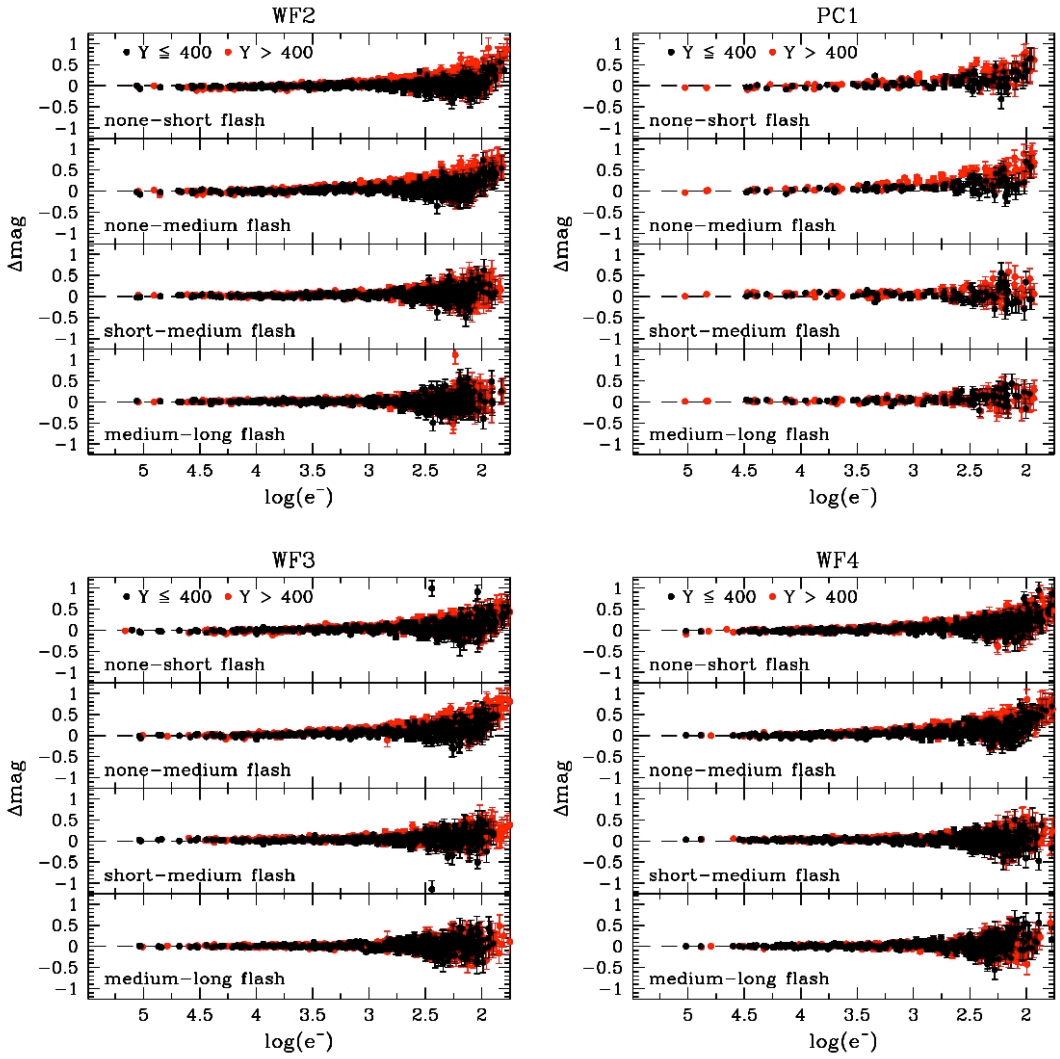

Figure 4. Same as Figure 3, but for stars imaged in the 100 s (ATD-GAIN=15) F814W exposures taken with common image orientations and the following combinations of INTFLAT ("flash") exposures: *(top panel of each plot)* no flash and short flash, *(second panel from top)* no flash and medium flash, *(second panel from bottom)* short flash and medium flash, and *(bottom panel)* medium flash and long flash.

Moreover, the mitigative effects are greater for star images that undergo a large number of vertical (parallel) charge transfers *(red points)* than those that undergo relatively few vertical charge transfers *(black points)*. The bottom panels in each plot show that the photometric benefit of background signal diminishes as the background signal increases. The convergence of the brightest stars (> 10^4 e^-) along the Δmag = 0 lines indicates that the CTI losses from such bright stars are relatively small and insensitive to the background signal.

Figure 4 shows similar plots for the four levels of INTFLAT illumination used for the 100 s (ATD-GAIN=15) external exposures obtained at both epochs (orientations). Again, the data are not CTI-corrected. The plots generally mimic those in Figure 3, except for the degree of photometric correction provided by the short and medium INTFLAT exposures on the magnitudes measured from the unflashed images. The corrections for stars fainter than ~1000 e^- are reduced by ~0.3 mag from the values noted above for the 14 s (ATD-GAIN=7) exposures. Moreover, these reductions affect mostly the star images located far from the horizontal (serial) registers of the CCDs *(red points)* than those closer to the horizontal registers *(black points)*. These phenomena can be seen by comparing the top two panels in each plot of Figure 4 with their counterparts in Figure 3. The reduced impact of the short and medium flashes is readily explained by the approximately six-fold increase in external sky background recorded in the 100 s external exposures over that recorded in the 14 s external exposures (Table 2). However, A/D quantization inconsistencies between the two ATD-GAIN settings may also be significant for the faintest stars.

We can quantify the photometric losses per vertical charge transfer near WFPC2's end-of-mission by examining the differences in the measured magnitudes of the same stars imaged at both field orientations (i.e., at two locations on each camera), as functions of star brightness and sky background. We ignore the horizontal charge-transfer losses, which were small and apparently independent of these factors (Dolphin 2009). Figures 5a and 5b show these relationships for our HSTphot measurements of the stars common to the WF2 images recorded at the two field orientations (Figure 2). We show the data from WF2 only, as they are typical of the data obtained from all four cameras. Each row of plots in Figures 5a and 5b represents the 14s (ATD-GAIN=7) and 100 s (ATD-GAIN=15) images obtained with similar levels of INTFLAT illumination.

Collectively, the plots in Figures 5a and 5b indicate that the logarithm of the charge lost from the small photometric apertures is linearly proportional to the number of vertical transfers of the charge packet toward the horizontal register, regardless of the strength of the source or background signals. The slope printed in each panel quantifies this behavior in term of photometric magnitude lost per vertical transfer. Figure 6 shows these slope values for all four WFPC2 cameras during the period April–August 2007, as functions of star and background signals. For faint stars (400–1000 e^-) and high background signals (~80 e^-) typically associated with long-exposure broadband WF images, approximately 16% of the integrated flux within the photometric aperture was lost over the maximum 800 vertical transfers. For similarly faint stars in narrow-band images that have little background signal, ~50–70% of the charge was lost when clocked along an entire column of the CCD.

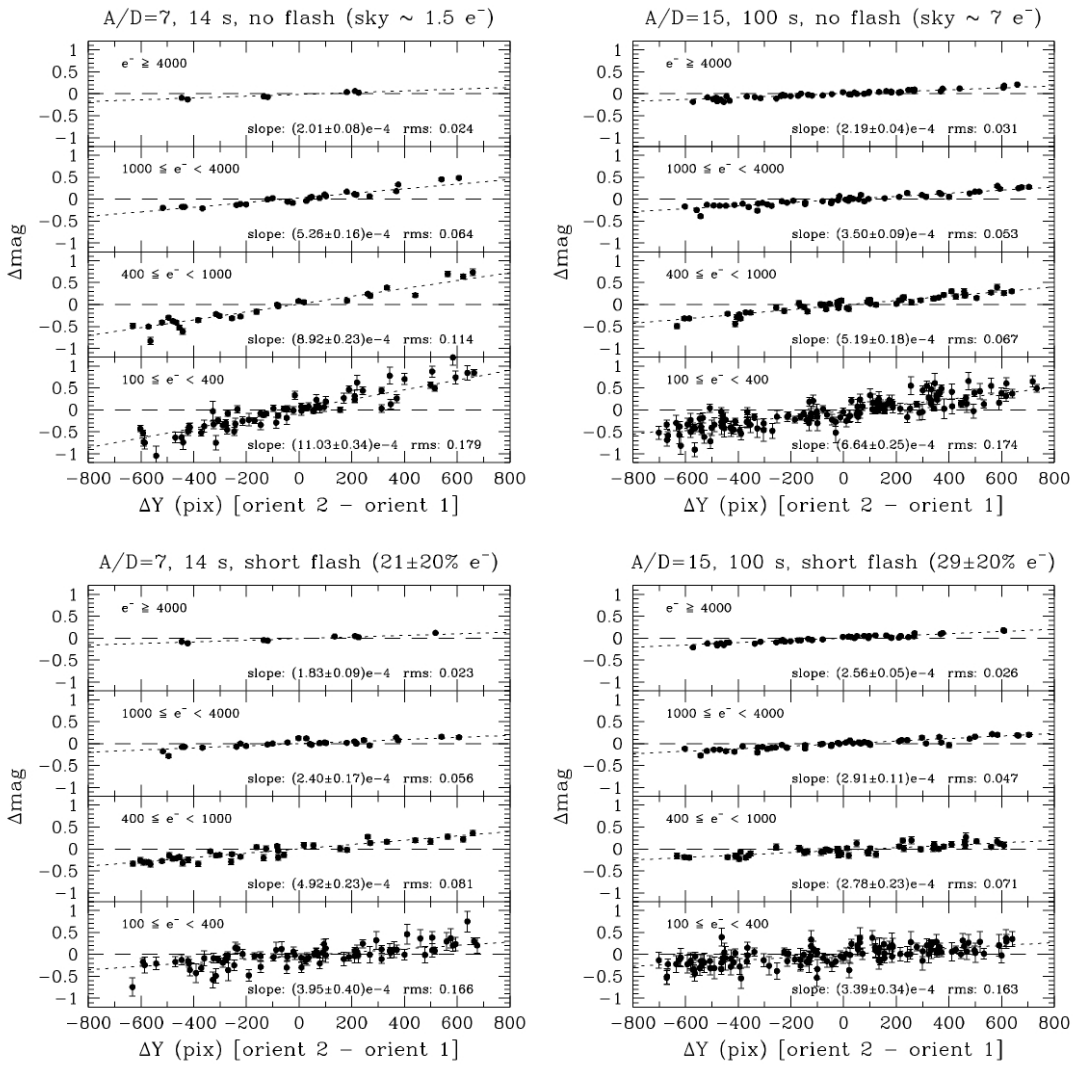

Figure 5a. Difference in F814W magnitudes (Δmag) of stars imaged at two field orientations (i.e., two detector locations) in the WF2 camera, as a function of the number of rows of pixels separating the images at each orientation. Each plot represents HSTphot measurements recorded for a particular combination of external and INTFLAT exposure times. *(Top row):* Data obtained from the *(left)* 14 s (ATD-GAIN=7) and *(right)* 100 s (ATD-GAIN=15) external exposures without INTFLAT illumination. *(Bottom row):* Data obtained from the 14 s and 100 s external exposures and short (3.5 s) INTFLAT lamp exposures. Each plot contains four panels that divide the data into four arbitrarily chosen bins of integrated star fluxes measured by HSTphot from the respective exposures. No CTI corrections have been applied. The parity of Δmag reflects the subtraction of the magnitudes obtained in April 2007 (orient 1) from those obtained in August 2007 (orient 2). The dashed line in each panel represents the linear least-squares fit to the data in that panel. The slopes of the lines and root-mean-squared deviations of the data from the lines are given in each panel.

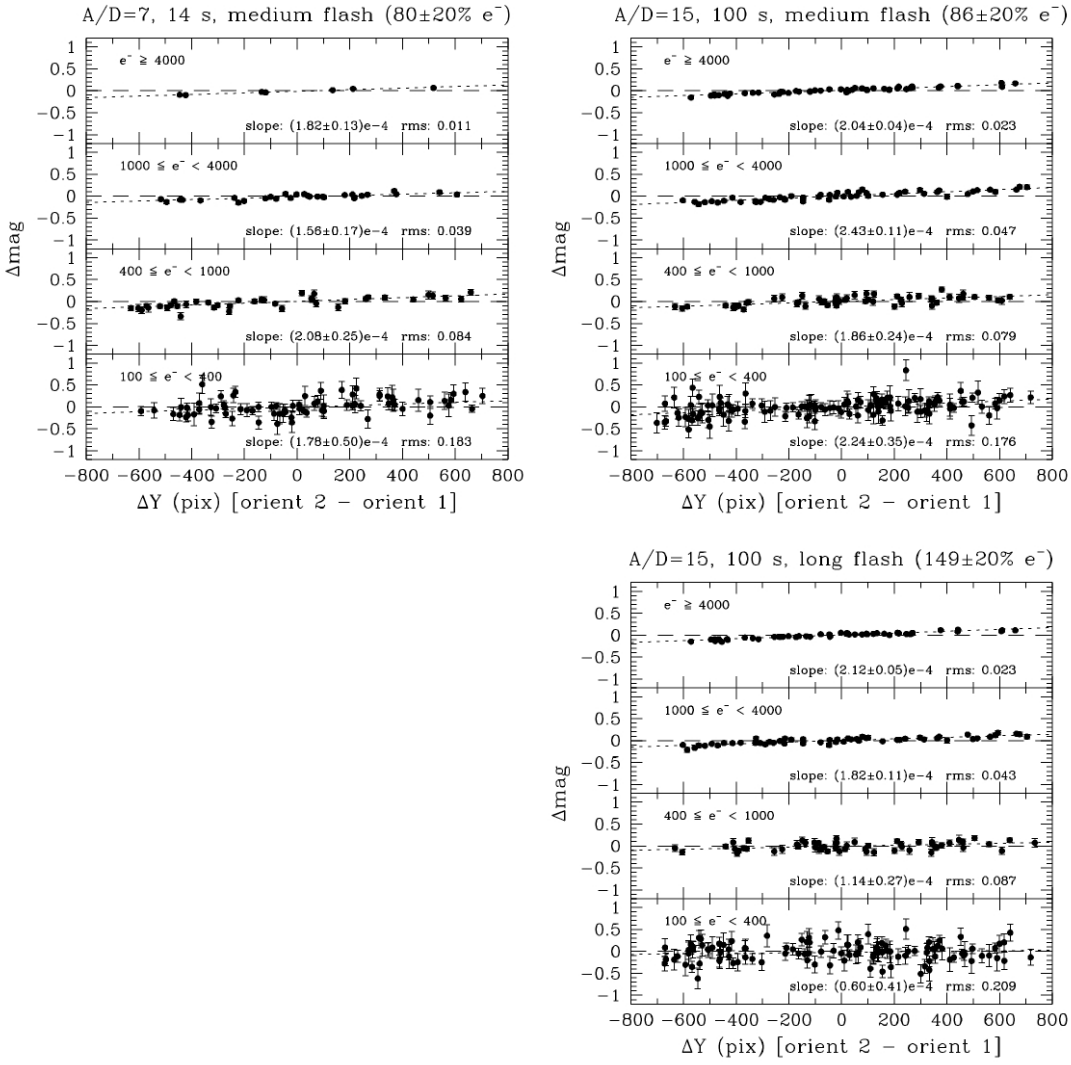

Figure 5b. Same as Figure 5a, but for WF2 images obtained with medium (14 s) INTFLAT exposures *(top row)* and long (28 s) INTFLAT lamp exposures *(bottom row)*. Note that long INTFLAT exposures were used only with the 100 s external exposures obtained with ATD-GAIN=15. The dimishing effect of CTI for fainter stars (100 ≤ e^- ≤ 1000) and larger background signals (> 80 e^-) suggests that most of the CTI mitigation is achieved when the background level becomes comparable to the average signal per pixel within the photometric aperture.

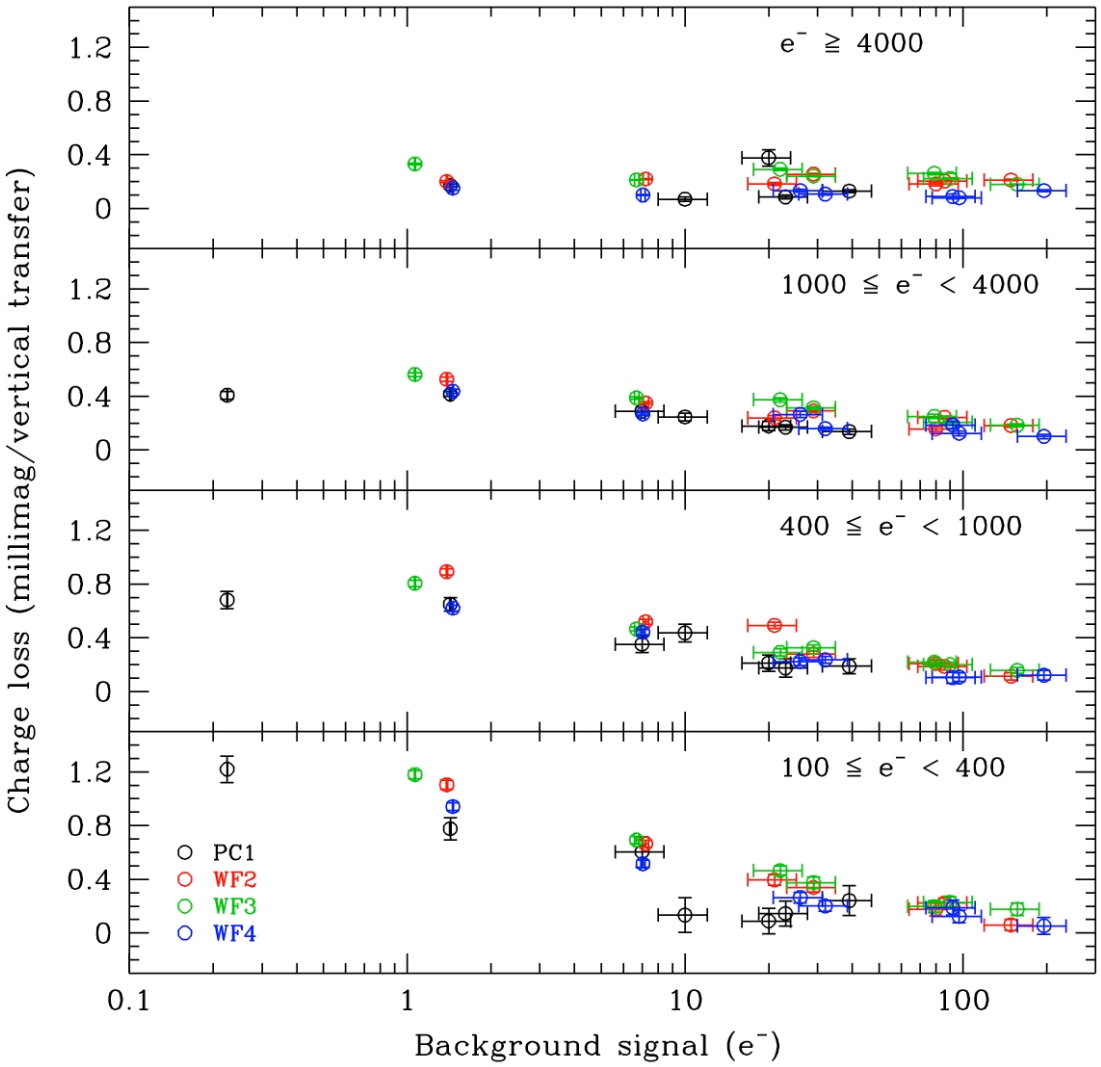

Figure 6. Charge lost from photometric aperture per vertical (parallel) transfer for each WFPC2 camera, as functions of star and background signal for the period April–August 2007. The panels correspond to the same ranges of integrated star flux shown in Figures 5a and 5b. The data points represent the slopes of the fitted lines shown in Figures 5a and 5b for WF2 (red points) as well as those computed (but not separately shown) for the other cameras (PC1 – black; WF3 – green; WF4 – blue).

Figure 6 shows similar, but not identical, CTE among the four WFPC2 cameras. For example, the WF4 points consistently lie on the low side of the locus of points representing all the cameras at comparable background signals. This trend indicates that (1) WF4 may have slightly better CTE than the other WFPC2 cameras, and (2) WF4 photometry obtained since Cycle 10 may be overcorrected by Dolphin's CTI correction formula, which is not calibrated against WF4 data obtained since the onset of WF4's amplifier anomaly in March 2002 (Biretta & Gonzaga 2005). Indeed, Dolphin has warned of possibly unreliable CTI corrections for WF4 data obtained after March 2002 (http://purcell.as.arizona.edu/wfpc2_calib/).

CTI correction of HSTphot and DAOPHOT photometry

We now examine the efficacy of the CTI-correction formula of Dolphin (2009) for the following three cases.

Case 1: HSTphot photometry + HSTphot CTI correction. CTI corrections are applied automatically by HSTphot v1.1 (updated 8 September 2009) to aperture-corrected fluxes obtained from *hstphot's* small-aperture photometry mode.

Case 2: HSTphot photometry + manual CTI correction. CTI corrections are applied subsequently to uncorrected HSTphot v1.1 photometry using a standalone version of Dolphin's CTI-correction formula.

Case 3: DAOPHOT photometry + manual CTI correction. CTI corrections are applied subsequently to DAOPHOT photometry using a standalone version of Dolphin's CTI-correction formula.

We assess these cases in the above order to progressively track the fidelity of the corrections produced from the native regime (HSTphot with internal CTI correction) to a mixed regime of a general-purpose photometry package with "manual" CTI correction.

Case 1. Figures 7a and 7b show the same WF2 data plotted in Figures 5a and 5b, respectively, after automatic correction of CTI by HSTphot. The slopes of the linear fits to the data in each panel represent the residual photometric error for the respective star and background signals. These residual photometric errors are plotted in Figure 8, along with those of the other three WFPC2 cameras.

Figure 8 shows that Dolphin's CTI correction (as applied by HSTphot) performs best on WF2 and WF3 photometry. For these cameras, the residual photometric errors are less than ~0.15 millimag per vertical transfer (hereafter abbreviated mmag/row) for all combinations of star and background signals. This value corresponds to a maximum error of ~0.06 mag for stars positioned at the centers of the WF2 and WF3 FOV. For

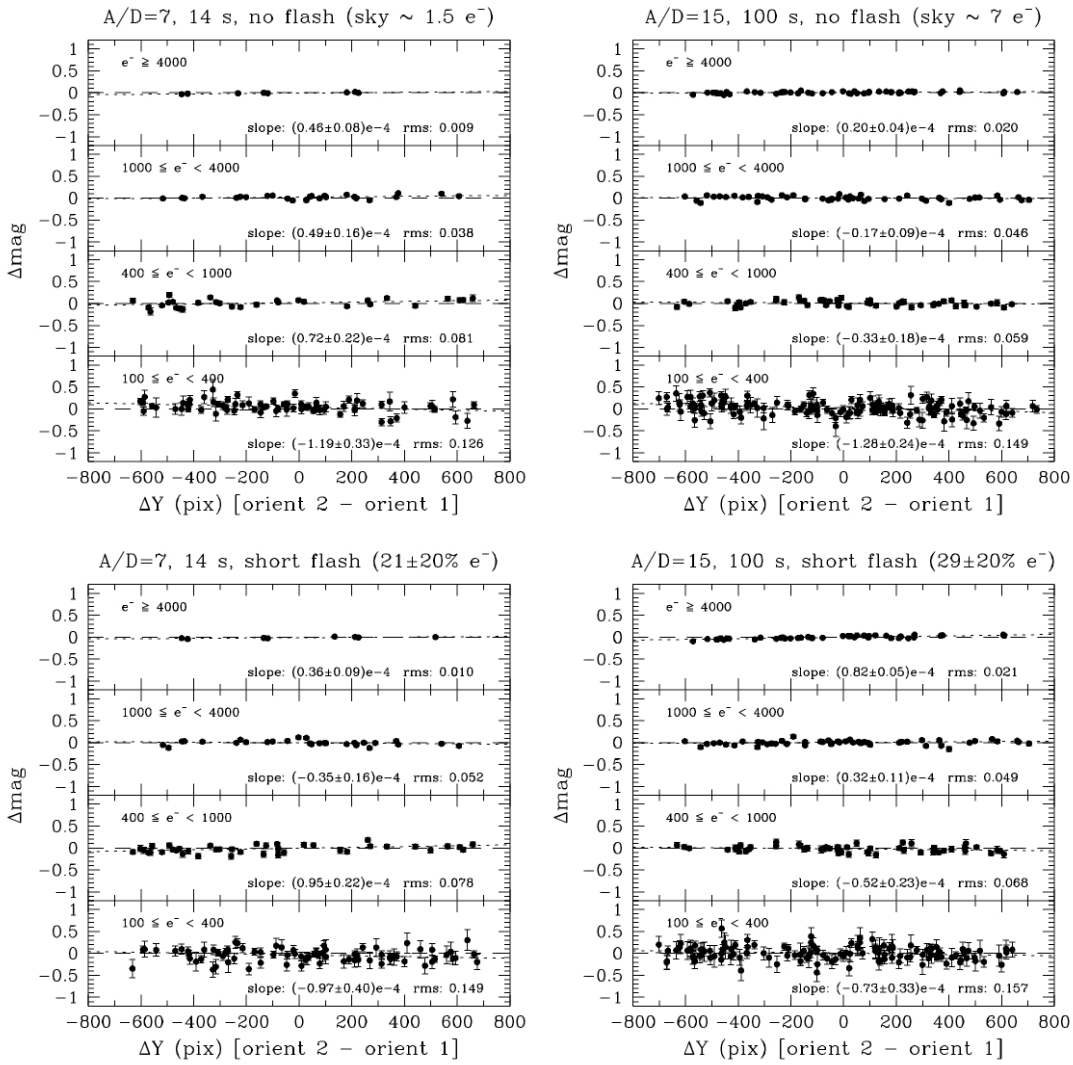

Figure 7a. Same WF2 data shown in Figure 5a, after automatic correction of CTI by HSTphot. The slopes of the linear fits to the data represent the residual photometric error in stellar magnitudes per vertical (parallel) charge transfer.

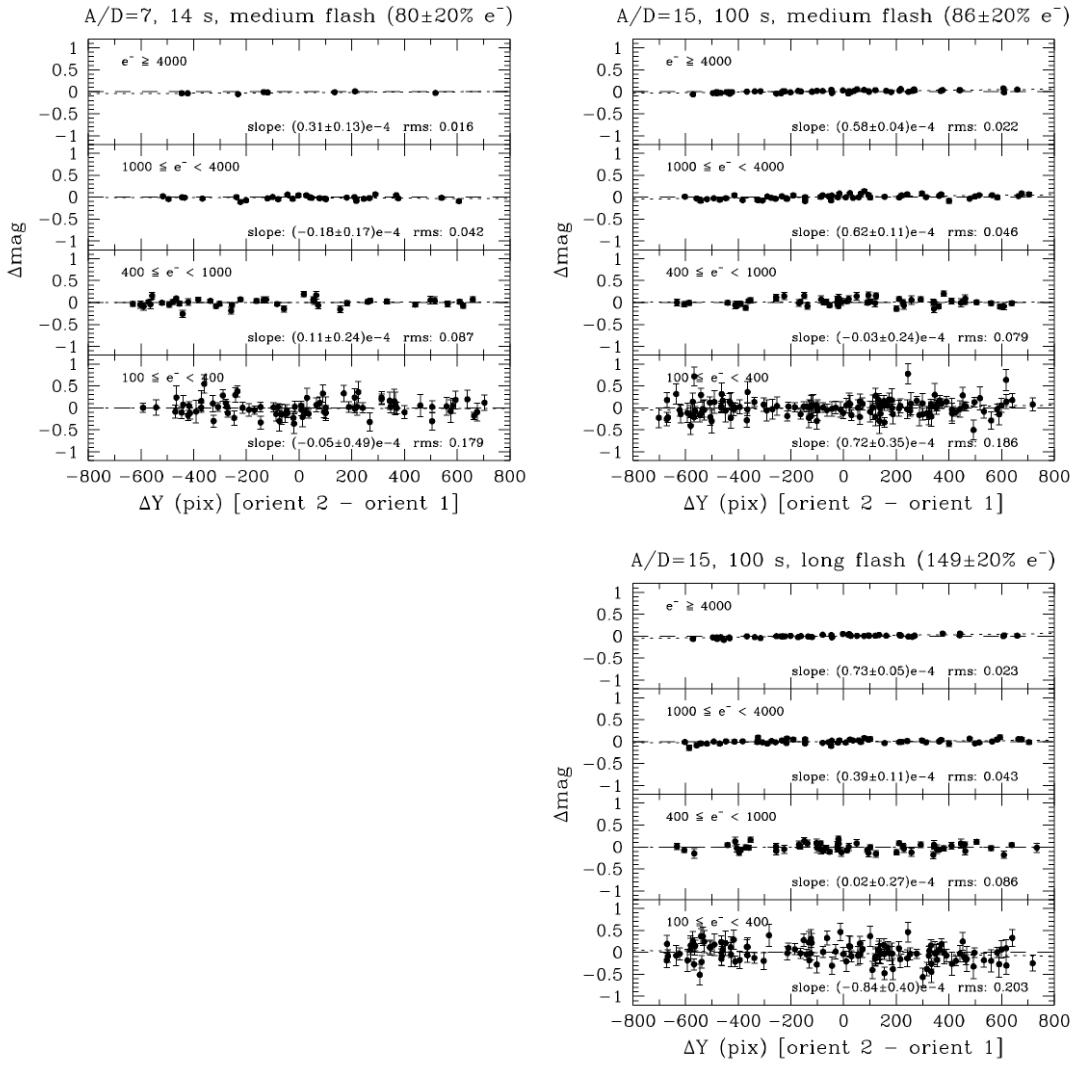

Figure 7b. Same WF2 data shown in Figure 5b, after automatic correction of CTI by HSTphot.

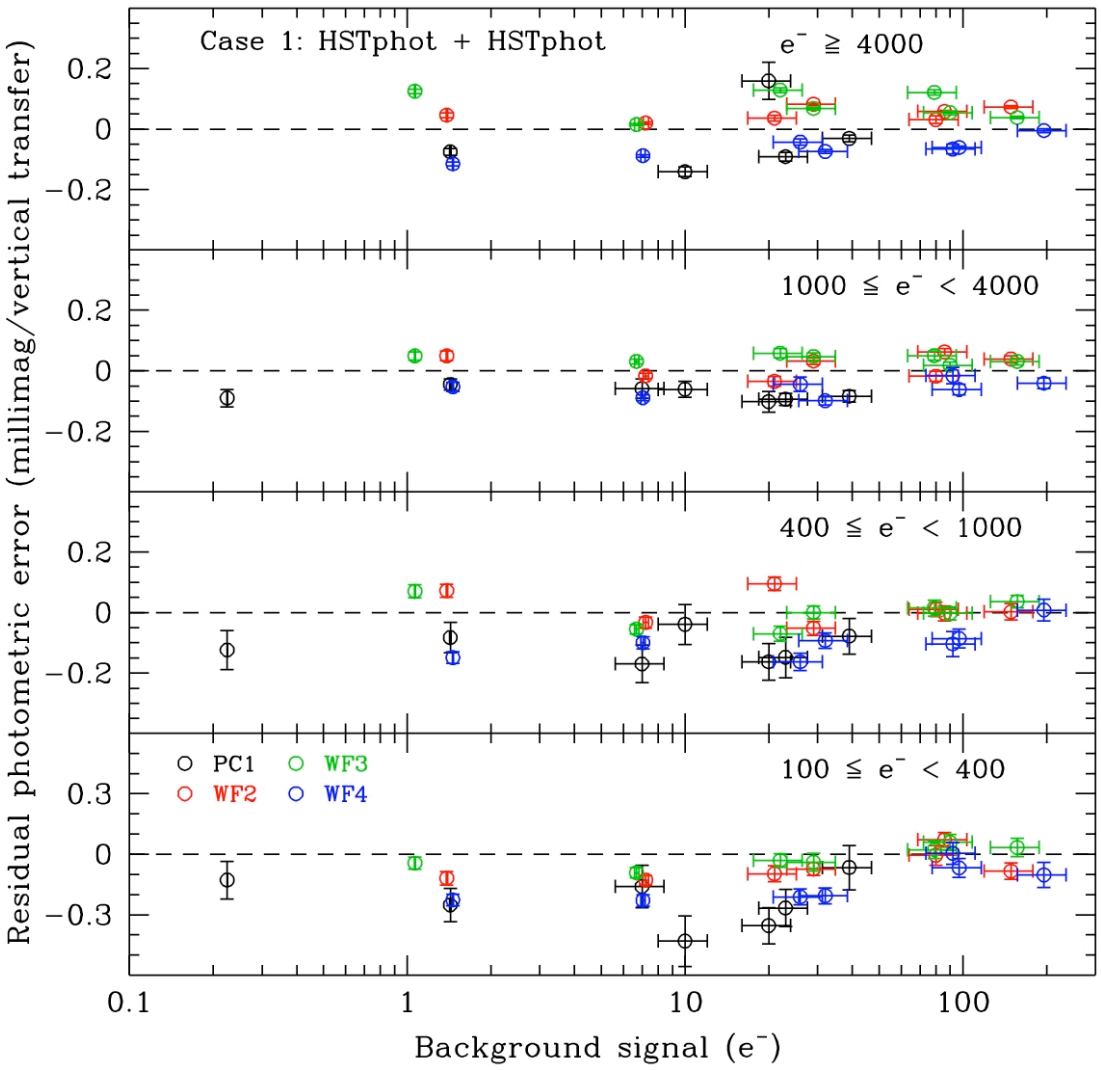

Figure 8. Residual photometric errors after automatic application of Dolphin's CTI correction to aperture magnitudes by HSTphot (Case 1). The panels correspond to the same ranges of integrated star flux shown in Figures 7a and 7b. The data points represent the slopes of the fitted lines shown in Figures 7a and 7b for WF2 (red points) as well as those computed (but not separately shown) for the other cameras (PC1 – black; WF3 – green; WF4 – blue).

stars of intermediate brightness (integrated fluxes of 400–4000 e^-), the residuals are symmetric about zero across the full range of background signals. However, HSTphot appears to undercorrect and overcorrect, respectively, the CTI of the brightest (≥ 4000 e^-) and faintest (≤ 400 e^-) stars by ~0.05 mmag/row (i.e., ~0.02 mag at the center of the FOV) for most background signals. The causes of these systematic errors are unknown, but they may be associated with image latency between successive non-dithered exposures of the brightest stars (McMaster & Biretta 2010) or selection effects involving widely separated pairs of the faintest stars (i.e., image pairs with large ΔY) whose differential photometry is sensitive to Poisson noise and/or extended trails of deferred charge from bright stars imaged at lower row positions.

HSTphot's CTI correction is less effective for PC1 and WF4 photometry of stars imaged over low-to-moderate background signals (< 50 e^-). Figures 6 and 8 show that the formula overcorrects the magnitudes of such stars by ~0.05–0.4 mmag/row, i.e., ~0.02–0.15 mag at the centers of the FOV. For moderate backgrounds, the over-correction is about twice the desired correction. These overcorrections may be due to the small number of PC stars used to calibrate the formula (because of the PC's small FOV) as well as Dolphin's exclusion of WF4 data from the calibration after March 2002. Because our April 2007 and August 2007 data were obtained soon after adjustments of the WF4 electronics temperature that temporarily remedied WF4's amplifier anomaly (Dixon et al. 2007), the results for WF4 shown in Figures 6 and 8 reflect the efficacy of HSTphot's correction of WF4 photometry in its least compromised state.

Case 2. Figure 9 shows the residual photometric errors after subsequent manual application of Dolphin's CTI correction to the aperture magnitudes generated by HSTphot. The plots are nearly identical to their counterparts in Figure 8. We traced the subtle inconsistencies between the two figures to small differences in the integrated aperture signals produced by HSTphot with and without the automatic corrections for CTI and photometric zero points. Our manual application of Dolphin's formula produces the same CTI corrections generated internally by HSTphot. This consistency allows us to investigate the compatibility of our standalone version of Dolphin's CTI correction with aperture magnitudes generated by other photometry packages.

Case 3. Figure 10 shows the residual photometric errors after subsequent application of our standalone version of Dolphin's CTI correction to the aperture magnitudes generated by DAOPHOT. (See the Data Processing section for the details of our DAOPHOT processing.) Although the DAOPHOT magnitudes were computed from aperture-corrected DAOPHOT fluxes, we sorted them for purposes of residual fitting and plotting according to their equivalent HSTphot integrated fluxes. Doing so enables consistency and fair comparison with Figure 8.

Two differences between the residual HSTphot and DAOPHOT errors are apparent. First, the DAOPHOT magnitudes of WF2 and WF3 sources are systematically over-corrected by ~0.1 mmag/row relative to their HSTphot counterparts for all combinations

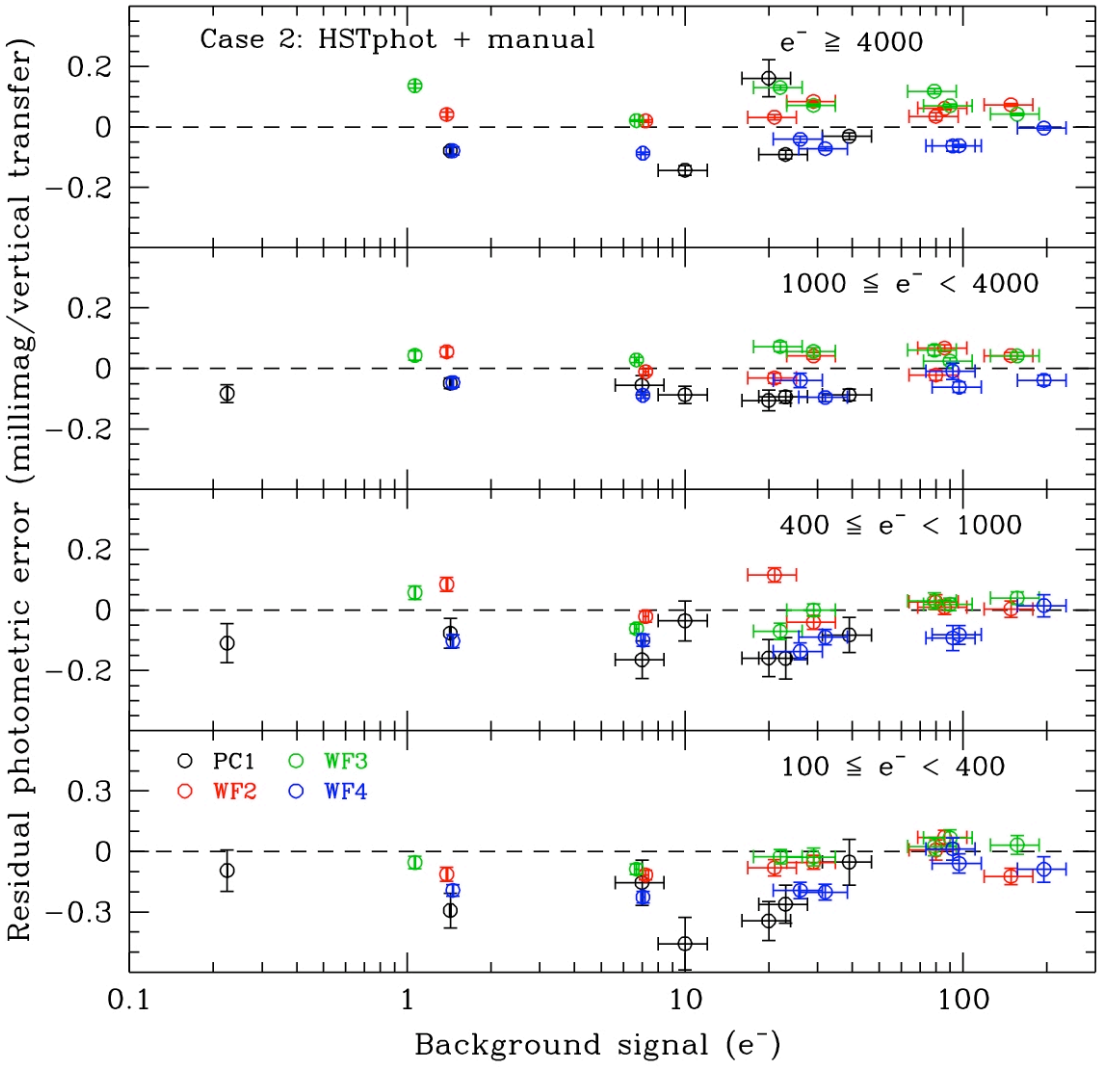

Figure 9. Residual photometric errors after subsequent manual application of Dolphin's CTI correction to aperture magnitudes computed by HSTphot (Case 2). The results are nearly identical to those shown in Figure 8 for Case 1.

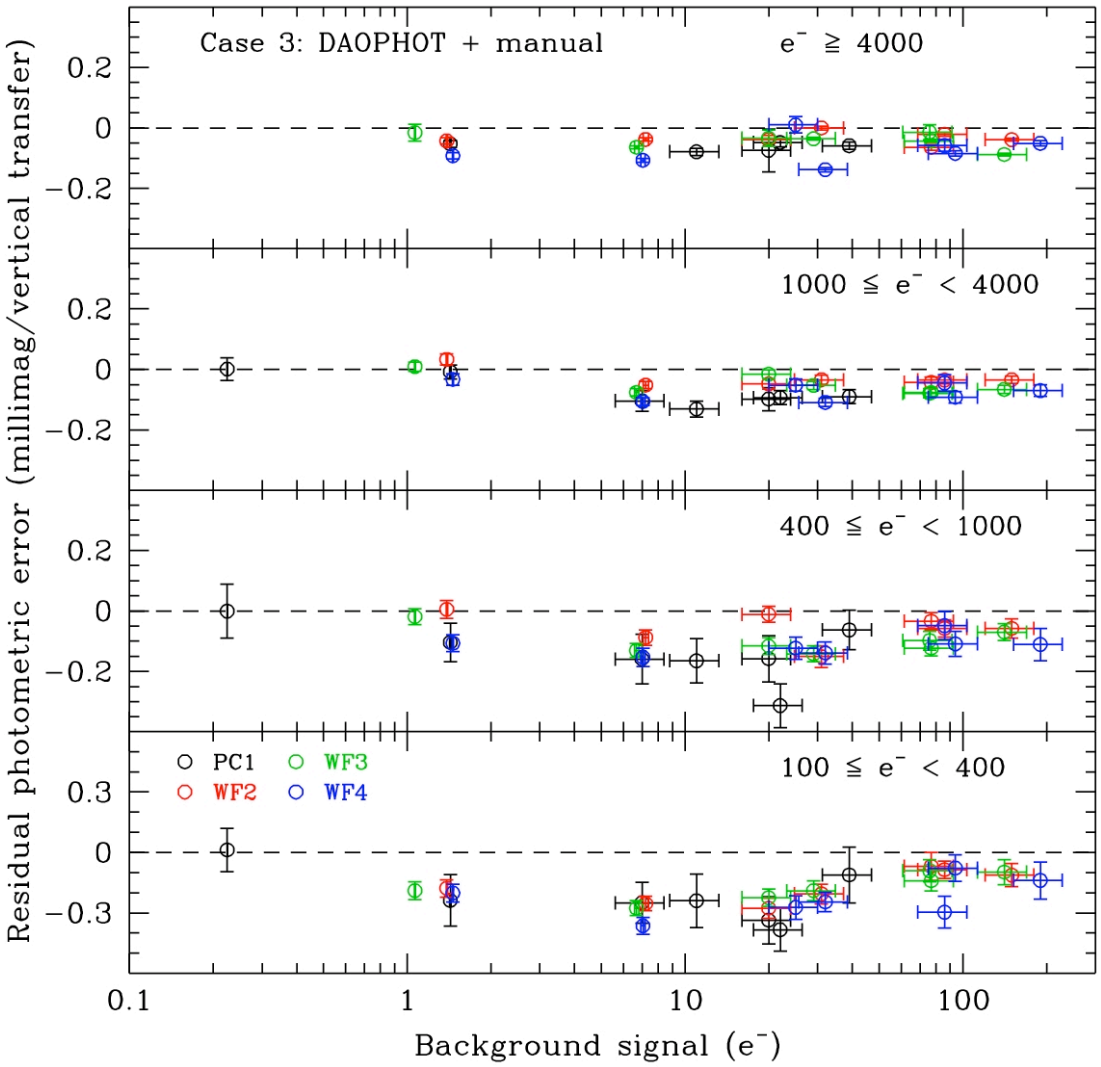

Figure 10. Residual photometric errors after subsequent manual application of Dolphin's CTI correction to aperture magnitudes computed by DAOPHOT (Case 3). To maintain consistency with the integrated flux bins used in Figures 5–9 for HSTphot photometry, the DAOPHOT fluxes were sorted according to their equivalent HSTphot values obtained by reducing the DAOPHOT fluxes by 33% (for the PC) and 29% (for the WF cameras). These scale factors reflect the effective differences between the algorithms used by DAOPHOT and HSTphot to perform circular aperture photometry over small regions of square pixels (see Page 9).

of star and background signals. On the other hand, the DAOPHOT and HSTphot results for PC1 and WF4 are formally indistinguishable because of larger measurement errors. Second, the dispersion of the DAOPHOT residuals for the combined cameras is ~0.05 mmag/row smaller than that of the HSTphot residuals for stellar fluxes greater than ~400 e^-. The causes of these effects are unclear, but the first one can be remedied simply by adding ~0.1y mmag to the CTI-corrected DAOPHOT magnitude, where y is the vertical coordinate of the star's position in the FOV. The second effect suggests that DAOPHOT's *phot* task, paired with the aperture corrections of Holtzman et al. (1995), is less sensitive to differences in image quality and sampling than HSTphot's small-aperture photometry mode.

Conclusions

We have examined the mitigative effect of background signal on the CTI of the WFPC2 detectors near the end of WFPC2's science mission using internally flashed images of a standard calibration field in ω Centauri obtained in April and August 2007. For faint stars (400–1000 e^-) and high background signals (~80 e^-) typically associated with long-exposure (~20 min) *V*-, *R*-, and *I*-band WF camera images, approximately 16% of the integrated flux within a circular aperture (r = 2 pix) was lost over the maximum 800 vertical charge transfers. For similarly faint stars in narrow-band images that have little background signal (< 10 e^-), about 50–70% of the charge was lost when clocked along an entire column of the CCD. Most of the CTI mitigation from uniform background illumination was attained when the background level was comparable to the average signal per pixel within the circular aperture. Higher background signals contribute only more photon noise to the photometric measurements. The CTI losses from stars with integrated aperture fluxes > 10^4 e^- were relatively small and insensitive to the background signal.

The CTE of the four WFPC2 CCDs were similar, but not identical, near the end of mission. For background signals > 10 e^-, WF4 exhibited better CTE than WF2 and WF3 at the statistically significant level of ~0.1 mmag/row (i.e., ~0.04 mag at the center of the FOV) for stars with integrated aperture fluxes > 100 e^-. This result is surprising given the often-assumed equality of the initial CTE of the Loral CCDs and their prolonged exposure to damaging on-orbit proton radiation. Nevertheless, our result is qualitatively consistent with earlier measurements of deferred-charge tails from hot pixels, which indicated that WF4's CTE was ~10% better than the CTE of the other WFPC2 CCDs in 2001 (Biretta & Kozhurina–Platais 2005). WF4's gain anomaly may cast suspicion on this result, but the close proximity of our calibration images to the March and August 2007 temperature adjustments that temporarily restored WF4's gain setting should have nullified any effect of the WF4 anomaly on our analysis (Dixon et al. 2007). Indeed, the photometry of stars imaged near the centers of WF2 and WF4 reveal no significant differences in the gains of those cameras at the epochs of our calibration images.

We have investigated the efficacy of the WFPC2 CTI-correction formula of Dolphin (2009) on aperture photometry obtained with the HSTphot and DAOPHOT software

packages. We note the following:

- Dolphin's corrections are most accurate for WF2 and WF3 photometry obtained with HSTphot. For these cameras, the residual photometric error is less than ~0.15 mmag/row for almost all combinations of star and background signals. This value corresponds to a maximum error of ~0.06 mag for stars positioned at the centers of the FOV. The residuals are symmetric about zero for stars of intermediate brightness (integrated fluxes of 400–4000 e^-), but HSTphot undercorrects and overcorrects, respectively, the CTI of brighter and fainter stars by ~0.05 mmag/row for most background signals.

- The CTI correction does not perform as well on PC1 and WF4 photometry of stars imaged over low-to-moderate background signals (< 50 e^-). The formula overcorrects the magnitudes of such stars by ~0.05–0.4 mmag/row, i.e., ~0.02–0.15 mag at the centers of the FOV. For moderate backgrounds, the overcorrection is about twice the desired correction. The overcorrection of WF4's magnitudes is not surprising given WF4's better CTE and Dolphin's exclusion of WF4 data obtained since March 2002 (the onset of the WF4 anomaly) from his CTI-correction calibration. The cause of the overcorrected PC1 magnitudes is unclear, but it may be due to the relatively small number of PC stars used to calibrate the CTI correction. On the other hand, the measurements of the deferred-charge tails from hot pixels indicate no significant differences among the CTE of PC1, WF2, or WF3 in 2001 (Biretta & Kozhurina–Platais 2005), so Dolphin's CTI correction should be well-suited to PC1 photometry despite being heavily weighted by WF2 and WF3 data after March 2002.

- The DAOPHOT magnitudes of stars imaged in WF2 and WF3 are overcorrected by ~0.1 mmag/row relative to their HSTphot counterparts for all combinations of star and background signals. The DAOPHOT and HSTphot results for PC1 and WF4 are formally indistinguishable, however, because of larger measurement errors. We find that DAOPHOT's integrated fluxes within 3-pixel (PC) and 2-pixel (WF) circular apertures are ~33% and ~29% larger, respectively, than those of HSTphot. These values diminish to ~1% and ~5% after applying the respective corrections for WFPC2's fiducial 0.″5 photometric aperture, so the overcorrections noted for WF2 and WF3 probably reflect small differences in DAOPHOT's and HSTphot's aperture summing and sky-subtraction algorithms.

- The dispersion of the CTI-corrected magnitude residuals for moderately bright stars (i.e., aperture fluxes greater than ~400 e^-) imaged in all the WFPC2 cameras is ~0.05 mmag/row smaller for DAOPHOT photometry than for HSTphot photometry. This suggests that DAOPHOT's *phot* task, paired with the aperture corrections of Holtzman et al. (1995), is less sensitive to differences in image quality and sampling than HSTphot's small-aperture photometry mode.

Recommendations

Although the systematic differences between our HSTphot and DAOPHOT results are small, we recommend that Dolphin's CTI correction be used in conjunction with aperture magnitudes derived from HSTPhot. This recommendation is particularly appropriate for WF2 and WF3 images obtained after March 2002 because the calibration of the CTI correction is heavily weighted by data from WF2 and WF3.

WF4's gain anomaly is well-corrected by the current version of *calwp2*. Nevertheless, the omission of WF4 data from Dolphin's calibration after March 2002 and WF4's apparently better CTE compel us to advise cautious use of Dolphin's correction with WF4 images obtained near the end of WFPC2's mission.

Users should also carefully check CTI-corrected PC photometry obtained with HSTphot. Our results show that the magnitudes of fainter stars (aperture fluxes < ~400 e^-) are significantly overcorrected when associated with moderate background signals (~10–50 e^-). Fortunately, only 12% of all archived WFPC2 images obtained with the PC1 or PC1-FIX apertures contain such background levels, so this problem should not be widely encountered.

Finally, users should beware that the quadratic time dependence of Dolphin's correction is a low-order fit to the magnitude losses from CTI over the lifetime of WFPC2. The short-term rates of WFPC2's CTE degradation have likely varied significantly in response to periodic and stochastic changes in solar activity (Fürst et al. 2009; Massey 2010). Because the results of this report are based on WFPC2 data obtained at effectively one observational epoch, any adjustments to CTI-corrected WFPC2 stellar photometry at other epochs that are inspired by this report should be applied with caution.

Acknowledgement

We gratefully acknowledge Andrew Dolphin for his assistance with HSTphot and his comments on the draft version of this report.

References

Biretta, J., & Gonzaga, S. 2005, Instrument Science Report WFPC2 2005-02 (Baltimore: STScI)

Biretta, J., & Kozhurina–Platais, V. 2005, Instrument Science Report WFPC2 2005-01 (Baltimore: STScI)

Dixon, V., Biretta, J., Gonzaga, S., & McMaster, M. 2007, Instrument Science Report WFPC2 2007-01 (Baltimore: STScI)

Dolphin, A. E. 2000a, PASP, 112, 1397

Dolphin, A. E. 2000b, PASP, 112, 1383

Dolphin, A. E. 2002, in *2002 HST Calibration Workshop*, eds. S. Arribas, A. Koekemoer, and B. Whitmore (Baltimore: STScI), p. 301

Dolphin, A. E. 2009, PASP, 121, 655

Fürst, F., Jörn, W., Rothschild, R. E., Pottschmidt, K., Smith, D. M., & Lingenfelter, R. 2009, E&PSL, 281, 125

Harris, H. C., Hunter, D. A., Baum, W. A., & Jones, J. H. 1993, AJ, 105, 1196

Holtzman, J., Hester, J. J., Casertano, S., Trauger, J. T., Watson, A. M., Ballester, G. E., Burrows, C. J., Clarke, J. T., Crisp, D., Evans, R. W., Gallagher, J. S., Griffiths, R. E., Hoessel, J. G., Matthews, L. D., Mould, J. R., Scowen, P. A., Stapelfeldt, K. R., & Westphal, J. A. 1995, PASP, 107, 156

Janesick, J. R. 2001, *Scientific Charge-Coupled Devices* (Bellingham: SPIE), p. 721

Jones, M. 2001, ACS Instrument Science Report 00-09 (Baltimore: STScI)

Massey, R. 2010, MNRAS, 409, L109

McMaster, M., & Biretta, J. 2010, Instrument Science Report WFPC2 2010-001 (Baltimore: STScI)

O'Dea, C., Mutchler, M., & Wiggs, M. 1999, Instrument Science Report WFPC2 1999-01 (Baltimore: STScI)

Stetson, P. B. 1987, PASP, 99, 191

Stetson, P. B. 1998, PASP, 110, 1448

Valdes, F. G., Campusano, L. E., Velasquez, J. D., & Stetson, P. B. 1995, PASP, 107, 1119

Walker, A. R. 1994, PASP, 106, 828

Whitmore, B., Heyer, I., & Casertano, S. 1999, PASP, 111, 1559